Numerical study of multiple periodic flow states in spherical Couette flow*

YUAN Li

ICMSEC & and LSEC, Academy of Mathematics and Systems Science,

Chinese Academy of Sciences, Beijing 100080, CHINA

Abstract

The supercritical flow states of the spherical Couette flow between two concentric spheres with the inner sphere rotating are investigated via direct numerical simulation using a three-dimensional finite difference method. For comparison with experiments of Nakabayashi *et al.* and Wimmer, a narrow gap and a medium gap with clearance ratio $\beta = 0.06$ and 0.18 respectively are considered for the Reynolds number range covering the first Hopf bifurcation point. With adequate initial conditions and temporary imposition of small wave-type perturbation, multiple periodic flow states with three different pair numbers of spiral Taylor-Görtler (TG) vortices have been simulated successfully for $\beta = 0.06$, of which the 1-pair and 2-pair of spiral TG vortices are newly obtained. Three different periodic flow states with shear waves, Stuart vortices or wavy outflow boundary, have been obtained for $\beta = 0.18$. Analysis of the numerical results reveals these higher flow modes in terms of fundamental frequency, wave number and spatial structure.

keywords: spherical Couette flow, non-unique flow solutions, spiral Taylor-Görtler vortices, shear waves, Stuart vortices.

1 Introduction

The spherical Couette flow (SCF) between two concentric rotating spheres gives rise to a rich variety of flow structures and instability mechanisms in the laminar-turbulent transition. Geometrically, a spherical shell can be considered as a combination of two other simpler systems with parallel disks in the pole region and cylindrical annulus near the equator, hence SCF is similar to the classical circular Couette flow near the equator, and to the flow between two rotating disks in a stationary casing near the pole. The study of SCF is of basic importance in providing insight into the physical mechanisms for the laminar-turbulent transition of a closed

---

rotating fluid, and is also relevant to astrophysical, geophysical and engineering applications due to spherical geometry and rotating motion [1].

In this paper we consider SCF with the inner sphere rotating and the outer sphere stationary. There are two control parameters that determine various flow regimes: a Reynolds number $Re = \Omega_1 R_1^2/\nu$ and a clearance ratio $\beta = (R_2 - R_1)/R_1$, with ν the kinematic viscosity, Ω_1 the angular velocity of the inner sphere, and R_1 and R_2 the radii of the inner and outer sphere. Various types of disturbance (flow structures, such as spiral TG vortices and travelling waves on toroidal vortices) and their characteristics (wavenumber, fundamental and rotational frequencies) strongly depend on the clearance ratio β [2, 3]. The Taylor instability in a form of axisymmetric toroidal Taylor vortices occurs as the first instability for narrow and medium gaps ($0 < \beta \leq 0.3$, as divided by Nakabayashi [3]), while the cross-flow instability in a form of periodic spiral waves (vortices) occurs as the first instability for wide gaps ($\beta > 0.3$) [4, 5]. An fascinating feature of SCF is that a variety of distinct unsteady disturbances with different wavenumbers or modulation patterns occurs as Re is increased, and some of which can exist at the same higher supercritical Re, in addition to the coexistence of multiple steady-state Taylor-vortex flows with different numbers of TG vortices at the same lower supercritical Re. This is related to bifurcation solutions of the Navier-Stokes equations in an enclose domain. In experimental studies of SCF, multiple flow states such as multiple steady TG vortex flows [6], multiple travelling waves on TG vortices [7, 8], and multiple shear waves with different wavenumbers and rotational frequencies [9], have been observed. In the numerical studies, on the other hand, multiple steady TG vortex flows have been simulated via time-marching calculations [10, 11, 12] or continuation methods [13, 14]. Numerical simulations of nonaxisymmetric disturbances such as spiral TG vortices and spiral waves were also conducted recently [5, 15, 16, 17]. The structure and formation mechanism of spiral TG vortices for $\beta = 0.14$ have been studied numerically recently by Sha and Nakabayashi [17]. However, simulations of multiple periodic disturbances with different pair numbers of spiral vortices or different wavenumbers have not been conducted for SCF.

The objective of the present study is to investigate the interesting multiple periodic flow solutions for narrow and medium gap cases that were observed in experiments [6, 8]. Particularly, three different periodic flow states with pair number of spiral TG vortices $S_\mathrm{P} = 1, 2$ and 3, are simulated at the same supercritical Re for $\beta = 0.06$, where only the branch $S_\mathrm{P} = 3$ was experimentally observed by Nakabayashi [3] and numerically simulated by Dumas [15]. We will show that the multiple spiral vortex flows can be easily calculated by temporary imposition of a wave-type perturbation. To further explore the structures of the multiple periodic solutions, a medium gap case with clearance ratio $\beta = 0.18$ is also studied, which corresponds to the experiment of Wimmer [6]. Shear waves, Stuart vortices and wavy outflow boundary at the equator were obtained in our simulation.

In the present study we utilized an artificial compressibility method in conjunction with a dual-time stepping technique for solving the unsteady 3D incompressible Navier-Stokes equa-

2

tions [18]. A third-order upwind compact finite difference scheme is used for the advective terms in this study. The resulting discretized equation is solved by a diagonalized ADI scheme. The method was tested to reproduce very well the steady-state TG-vortex flows with vortex cell number $N = 0, 2$ and 4 for $\beta = 0.18$ [12]. In this paper we specifically focus on multiple periodic flow states at higher Re.

2   Mathematical Formulation and Numerical Method

Consider an annulus between two concentric spheres filled with an incompressible Newtonian fluid of constant density and kinematic viscosity ν. The inner sphere is constrained to rotate about the vertical axis with a prescribed angular velocity Ω_1. To implement the artificial compressibility method, the incompressible Navier-Stokes equations are written in conservative form in generalized coordinate system with pseudo-time derivatives added:

$$\frac{\partial \hat{\mathbf{Q}}}{\partial \tau} + \mathbf{I}_m \frac{\partial \hat{\mathbf{Q}}}{\partial t} + \frac{\partial (\hat{\mathbf{E}} - \hat{\mathbf{E}}_\nu)}{\partial \xi} + \frac{\partial (\hat{\mathbf{F}} - \hat{\mathbf{F}}_\nu)}{\partial \eta} + \frac{\partial (\hat{\mathbf{G}} - \hat{\mathbf{G}}_\nu)}{\partial \zeta} = 0, \tag{1}$$

where $\hat{\mathbf{Q}} = \mathbf{Q}/J = (p, u, v, w)^{\mathrm{T}}/J$, $\mathbf{I}_m = \mathrm{diag}(0, 1, 1, 1)^{\mathrm{T}}$, J is the Jacobian of the coordinate transformation, p is the pressure, u, v and w are the Cartesian velocity components, τ and t are the pseudo-time and physical time, respectively, $\hat{\mathbf{E}}, \hat{\mathbf{F}}, \hat{\mathbf{G}}$ are the inviscid flux vectors, and $\hat{\mathbf{E}}_\nu, \hat{\mathbf{F}}_\nu, \hat{\mathbf{G}}_\nu$ are the viscous flux vectors (cf.ref.[19]). Note that a subiteration is needed at each physical time step to drive the artificial compressibility terms toward zero to satisfy the continuity equation.

Applying an implicit backward difference to the pseudotime derivatives , a second-order, three point backward difference to the physical time derivatives, a first-order flux-difference splitting to the advective terms of the LHS, and the diagonalized Beam-Warming scheme, one obtains [18]

$$\mathbf{T}_\xi \left[\mathbf{D} + \delta_\xi^- \mathbf{\Lambda}_\xi^+ + \delta_\xi^+ \mathbf{\Lambda}_\xi^- - \delta_\xi \mathbf{A}_\nu' \bar{\delta}_\xi \right] \mathbf{T}_\xi^{-1} \mathbf{D}^{-1} \mathbf{T}_\eta \left[\mathbf{D} + \delta_\eta^- \mathbf{\Lambda}_\eta^+ + \delta_\eta^+ \mathbf{\Lambda}_\eta^- - \delta_\eta \mathbf{B}_\nu' \bar{\delta}_\eta \right]$$

$$\times \mathbf{T}_\eta^{-1} \mathbf{D}^{-1} \mathbf{T}_\zeta \left[\mathbf{D} + \delta_\zeta^- \mathbf{\Lambda}_\zeta^+ + \delta_\zeta^+ \mathbf{\Lambda}_\zeta^- - \delta_\zeta \mathbf{C}_\nu' \bar{\delta}_\zeta \right] \mathbf{T}_\zeta^{-1} \Delta \mathbf{Q}^{n+1,m} = - \left[\partial_\xi \hat{\mathbf{E}} + \partial_\eta \hat{\mathbf{F}} + \right.$$

$$\left. \partial_\zeta \hat{\mathbf{G}} - \delta_\xi \hat{\mathbf{E}}_\nu - \delta_\eta \hat{\mathbf{F}}_\nu - \delta_\zeta \hat{\mathbf{G}}_\nu \right]^{n+1,m} - \frac{\mathbf{I}_m}{\Delta t} \left(1.5 \hat{\mathbf{Q}}^{n+1,m} - 2 \hat{\mathbf{Q}}^n + 0.5 \hat{\mathbf{Q}}^{n-1} \right), \tag{2}$$

where $\mathbf{D} = \frac{1}{J} \left(\frac{1}{\Delta \tau} + \frac{1.5}{\Delta t} \right) \mathbf{I}$, $\mathbf{I}$ is the identity matrix, δ^+, δ^- and δ ($\bar{\delta}$) are forward, backward and central (midpoint central) differences, respectively, $\mathbf{A}_\nu' = \frac{1}{Re} (\bigtriangledown \xi \cdot \bigtriangledown \xi) \mathbf{I}$ is the modified orthogonal part of viscous terms, $\mathbf{T}_\xi^{-1}, \mathbf{T}_\xi$ and $\mathbf{\Lambda}_\xi$ are the left and right eigenvector matrices and eigenvalues of the Jacobian $\mathbf{A} \equiv \partial \hat{\mathbf{E}} / \partial \mathbf{Q}$, and $\mathbf{\Lambda}_\xi^\pm = \frac{1}{2} (\mathbf{\Lambda}_\xi \pm |\mathbf{\Lambda}_\xi|)$ (cf.ref.[18]). The third-order upwind compact scheme is applied to the discretization of the advective terms in the RHS of Eq.(2) dimension by dimension:

$$\partial_\xi \hat{\mathbf{E}} + \partial_\eta \hat{\mathbf{F}} + \partial_\xi \hat{\mathbf{G}} = \mathbf{A} \partial_\xi \mathbf{Q} + \mathbf{B} \partial_\eta \mathbf{Q} + \mathbf{C} \partial_\zeta \mathbf{Q}, \tag{3}$$

3

where $\mathbf{A}\partial_\xi\mathbf{Q} = \mathbf{A}^+(\partial_\xi\mathbf{Q})^+ + \mathbf{A}^-(\partial_\xi\mathbf{Q})^-$, $\mathbf{A}^\pm = \mathbf{T}_\xi\mathbf{\Lambda}_\xi^\pm\mathbf{T}_\xi^{-1}$, and the upwind-biased difference $(\partial_\xi\mathbf{Q})^\pm$ can be computed by a third-order upwind compact finite difference scheme [12].

In the calculation, the computational domain of the spherical shell is divided into a number of grids in the radial (r), meridional(θ) and azimuthal (ϕ) directions, respectively. The grids are uniform in θ and ϕ directions, but are clustered near the wall of two spheres in the radial direction. Referring a recent finite-difference simulation of the spiral TG vortex flow for $\beta = 0.14$ [17] where a grid of $22 \times 361 \times 91$ was found sufficient to resolve the spiral TG vortex flow, a grid with $21 \times 361 \times 89$ grid points is used for the narrow gap ($\beta = 0.06$), and that with $31 \times 361 \times 129$ is used for the medium gap ($\beta = 0.18$) in this work. For subcritical Re numbers, the calculations were initiated from the Stokes flow and marched in pseudo-time only. For supercritical Re numbers, however, low-Re flow fields were used for initialization in order to avoid excessive computational times for initial transients. For all unsteady simulations the physical time step is $\Delta t = 0.01\Omega_1^{-1}$. The subiteration for unsteady computation is thought as converged when L_2 norm of the residuals has been reduced 10^{-2} from its initial value [18]. After the initial transients have died out, this level of convergence is achieved within 5-15 subiterations per physical time step.

Non-slip conditions are applied to velocities, and the pressure is obtained by the momentum equation in the radial direction on both spheres. The polar boundary is treated as in ref.[18]. A reference pressure is taken at a specified point in the interior domain.

3   Routes to supercritical non-unique flow states

The solution of the incompressible Navier-Stokes equations for an arbitrary bounded fluid is unique and unconditionally stable only at low Re (cf. [20]), whereas bifurcation solutions may occur for $Re \geq Re_c$ with Re_c being the first critical Reynolds number. This is generally true for rotating fluid in an enclosed cavity volume. A branch of bifurcation solutions is either stable or unstable, and can exist only within a certain subset of control parameter space. In experiments it was observed that the formation of multiple flow states strongly depends on the initial flow state and on the control parameter evolution history [6, 8]. In numerical computation of bifurcation solutions via time marching scheme, it is found that other factors can also affect the development of multiple flow states. These factors include the form of artificial perturbation added, its magnitude and imposing duration. It is a rule of thumb that while arbitrarily large perturbation may be imposed in calculating steady-state flow where physical dissipation is sufficiently large to dampen out artifacts, small perturbation must be used as shortly as possible in calculating unsteady flow state. The temporary imposition of small artificial perturbation is reasonable in a sense that actual flow system usually may experience some imperfection such as rotation whim in SCF. The perturbation often plays an important role in receptivity of flow instability or mode selection among bifurcation solutions, due to sensitivity of bifurcation. It accelerates the instability for linearly instability or helps selection of flow mode for nonlinear

instability. To get a whole picture of bifurcation solutions, a genetic bifurcation method such as the continuation method is necessary, but it is computationally expensive for obtaining time-dependent bifurcation solutions. In this paper, a wave-form perturbation that was used by Schroeder and Keller [21] to trigger travelling waves in circular Couette flow,

$$
\begin{aligned}
v_r &= -4\epsilon_1 \frac{(r-R_1)(r-R_2)}{\beta^2} \cos\left[\pi\left(1 - \frac{2z}{G} - \epsilon_2\alpha\right)\right] \\
v_\theta &= \epsilon_1 \sin\left[\frac{\pi}{2}\frac{(r-R_1)(r-R_2)}{\beta^2}\right] \sin\left[\pi\left(1 - \frac{2z}{G} - \epsilon_2\alpha\right)\right]\frac{R_1}{\beta} \\
\text{with} \quad z &= R_2(\frac{\pi}{2} - \theta), \qquad \alpha = \sin(m_a\phi), \qquad G \approx 2\beta, \qquad \epsilon_2 = 0.4
\end{aligned}
\tag{4}
$$

is imposed for a period of viscous diffusion time defined as $t_d = (R_2 - R_1)^2/\nu$. The viscous diffusion time is related to the development of the TG vortices, because that development is due to diffusion of the vorticity produced by the inner-sphere rotation. The amplitude of perturbation ϵ_1 in Eq.(4) in the range of $10^{-4} \sim 10^{-6}$ is found to lead to sufficient instability yet not artificially distort the flowfield much.

4   Results

The clearance ratios for the narrow gap and the medium gap, $\beta = 0.06$ and 0.18, are the same as those in experiments [2] and [6], respectively. The Reynolds number is confined to $Re \leq 3800$ for $\beta = 0.06$ and $Re \leq 8000$ for $\beta = 0.18$. For convenience of discussion, notations used by Nakabayashi [3] is adopted here. The flow regime is characterized by "flow region I, II, III and IV" + "kinds of disturbances", where the flow region I is a laminar basic-flow region, region II is TG vortex-flow region, region III is a transition region, and IV is a turbulent flow region. The kinds of disturbances refer to vortices and waves of the flow, such as TG vortex (T), spiral vortex (S), travelling waves (W), shear waves (S_h), Stuart vortices (S_u), etc. The flow regime is classified by the flow state expressed by the cell number of toroidal TG vortices N (the pair number $N/2$), the pair number of spiral TG vortices S_P and the wavenumber of travelling waves on TG vortices m, that of shear waves S_H or Stuart vortices S_U. For example, IITS($N = 2, S_P = 3$) refers to the spiral TG vortex flow. Present attention is focused on multiple periodic flow states in flow regime II that occurs after Hopf bifurcation.

4.1   Narrow gap $\beta = 0.06$

For this narrow gap case, cylinder-like disturbances such as spiral TG vortices and travelling waves on TG vortices play an important role [3]. We will show that both multiple steady-state solutions and multiple periodic solutions exist for $\beta = 0.06$.

Firstly, we computed the basic flow state IB($N = 0$) at $Re = 2767$. The Reynolds number was then increased with $\Delta Re = 100$ to detect when Taylor vortex will occur. The simulation of the 2-vortex flow IIT($N = 4$) at $Re = 3067$ is quite straightforward. It is found that the

2-vortex flow exists stably for $3020 \leq Re \leq 3130$. To obtain the 1-vortex flow that may need symmetry-breaking bifurcation [11], we impose artificial initial condition. In the initial stage of the diffusion time t_d long, two artificial radial dividing lines are placed at one gap-width away from the equator on northern and southern sides respectively, and symmetry condition is artificially used with respect to each line. A crude "1-vortex" flow state with an inflow boundary at the equator is thus produced between each dividing line and the equator. After the dividing line is removed, the flow settles down to steady-state 1-vortex flow IIT($N = 2$). Figure 1 shows these two steady flows. By quasi-statically changing Re, it is found that the 1-vortex flow exists stably for $2980 \leq Re < 3080$, thus giving a small overlap range $3020 \leq Re \leq 3080$ where two steady-state flows coexist. This feature is consistent with that for a medium gap $\beta = 0.18$ [11, 12]. The computed first critical $Re_c = 2980$ is very close to 2979 given by empirical formula [7]: $Re_c = 41.3(1 + \beta)\beta^{-\frac{3}{2}}$, though larger than 2760 of [2].

Secondly, by using the 1-vortex flow at $Re = 3080$ as initial flowfield and quasi-statically increasing Re slightly above $Re = 3140$, the flow becomes singly periodic due to Hopf bifurcation (secondary instability). It undergoes an intermediate stage with axial symmetry but equatorial asymmetry. The cell number of toroidal TG vortices varies between 2 and 4. The intermediate state can remain unchanged for several hundred inner-sphere revolutions without artificial perturbation, but it is unstable to the perturbation (4), and ultimately evolves into the supercritical spiral TG-vortex flow IITS. It is found that $Re \approx 3140$ is the second critical Reynolds number Re_s for the occurrence of spiral TG vortices. The present value of $R^\star = Re_s/Re_c = 1.05$ is slightly smaller than experimentally estimated value $R^\star = 1.08$ [3].

The multiple spiral TG vortex flows IITS with three different pair number of spiral vortices ($S_P = 1, 2$ and 3) can be simulated using $m_a = 1, 2$ and 3 in Eq.(4). The duration of the perturbation is the viscous diffusion time τ_d or shorter. Figure 2 shows the three flow states at $Re = 3300$. The existence of $S_P = 3$ flow has been verified by experiment [2]and numerical simulation [15]. The occurrence of newly simulated $S_P = 1$ and 2 flow states seems reasonable in the sense that they are obtained with identical condition with $S_P = 3$ except with different m_a. Once the flow states are formed, they are stable in the range $3140 \leq Re \leq 3800$, and further imposition of perturbation (4) with different m_a does not push them out of the corresponding state. We have tested using $m_a = 1 \sim 11$, only the above three flow states can be obtained. Regarding the structure of the spiral TG vortex flow, it can be seen from Fig. 2 that each flow consists of one toroidal TG vortex and S_P pair of spiral vortices in each hemisphere. Figure 3 shows the time history of circumferential velocity component v_θ at the equator in the central spherical surface of the gap. The periodicity corresponds to the fundamental frequency f_S, which represents the frequency of the disturbance passing a fixed point in the laboratory reference frame. The rotational frequency of the branch IITS ($S_P = 3$), defined as f_S/S_P, is $0.467 \, \Omega_1$ at $Re = 3300$, in good agreement with experiment [3] and calculation [15].

As regard to the formation mechanism of spiral vortices, Ref.[17] revealed that the vorticity tilting is responsible for generating the spiral vortices, and vorticity stretching acts to stretch

6

one of the spiral vortices and suppress the stretching of the other in the azimuthal direction. We do not perform similar analysis and simply presume that their conclusion can also be applied to the generation of the spiral vortices for $\beta = 0.06$. Nevertheless, the vorticity tilting is found to develop from growth of wave-form perturbation.

4.2   Medium gap $\beta = 0.18$

For this medium gap case, disk-like disturbances such as shear waves and Stuart vortices occur at high Re and exist together with each of the different TG vortex flows near the equator. The phenomenon that multiple steady-state and unsteady solutions exist was observed in experiments [6, 8] for $\beta = 0.18$, but numerical simulation of high-mode disturbances has not been done before. Our numerical simulation will show that multiple solutions at high Re are variations of multiple TG vortex flows at low Re superposed by disk-like disturbances such as shear waves or Stuart vortices.

In a previous study for $\beta = 0.18$, we have found that steady-state supercritical 0-, 1-, and 2-vortex flows coexist in the range of $Re \geq 1220$ [12]. Using the three flow states as initial conditions, multiple periodic solutions can be obtained at the same supercritical Re number (say $Re = 7200$). Figure 4(a) shows the 2-vortex flow with eight shear waves: $\text{IITS}_\text{h}(N = 4, S_\text{H} = 8)$. The outflow boundary of the toroidal TG vortex become wavy due to interaction with the shear waves. The shear waves look like spiral vortices, and are thought to result from the viscous cross-flow instability [3]. Fig. 4(b) shows 1-vortex flow with five Stuart vortices: $\text{IITS}_\text{u}(N = 2, S_\text{U} = 5)$. Fig. 4(c) shows the zero-vortex flow with eight shear waves: $\text{IITS}_\text{h}(N = 0, S_\text{H} = 8)$. The outflow boundary at the equator is wavy. There is difference between Stuart vortices and shear waves. The shear waves are similar to spiral vortices in the narrow gap case, as both have a counterclockwise spirals from high latitude region to the equator when viewing from top of the north pole, but are different in that the shear waves are more extensive into high latitude region and more tilted with respect to the azimuthal direction, and most of all, there is no discernible vortex cell across the whole gap. The shear waves are also found for a wide gap in a previous study (called spiral waves in [5]). The Stuart vortices in Fig. 4(b) have clockwise spirals and do not extend to the equatorial region so that the outflow boundary of toroidal TG vortex is still horizontal. The isosurfaces of the meridional velocity magnitude in Figure 5 reveal that the shear waves extend from the north polar region to the equatorial region in counterclockwise direction (Fig. 5(a)), while the Stuart vortices are in clockwise direction (Fig. 5(b)). These disturbances are essentially periodic at this Re.

5   Conclusions

The non-unique periodic flow states of the spherical Couette flow are simulated by solving the unsteady three-dimensional incompressible Navier-Stokes equations using a third order upwind compact finite difference method. The numerical results reveal that two spiral TG vortex flows

with pair number 1 and 2 coexist in addition to the well known $S_{\mathrm{P}} = 3$ spiral TG vortex flow at low supercritical Reynolds number for the narrow gap $\beta = 0.06$. The development of bifurcation solutions is shown to depend on the wavenumber of the artificial perturbation, besides on the number of toroidal vortices in initial flow mode and Reynolds number evolution history. It is also found that multiple steady Taylor-Görtler vortex flows at low Re evolve into multiple periodic flow states at higher Re (say 7200) for $\beta = 0.18$. The 2-vortex flow and 0-vortex flow develop shear waves ($S_{\mathrm{H}} = 8$) and both have wavy outflow boundaries, while 1-vortex flow develops Stuart vortices ($S_{\mathrm{U}} = 5$). The numerical results are in qualitative agreement with previous experiments.

6   Acknowledgements

References

[1] Wimmer M. Viscous flow and instabilities near rotating bodies. Prog. Aerospace Sci. 1988, **25**:43-103.

[2] Nakabayashi K. Transition of Taylor-Görtler vortex flow in spherical Couette flow, J. Fluid Mech., 1983, **132**:209-230.

[3] Nakabayashi K, Tsuchida K and Zheng Zhiming. Characteristics of disturbances in the laminar-turbulent transition of spherical Couette flow, part 1 & 2. Phys. Fluids, 2002, **14** (11):3963-3982.

[4] Egbers C and Rath H J. The existence of Taylor vortices and wide-gap instabilities in spherical Couette flow. Acta Mech., 1995, **111**:125-140.

[5] Araki K, Mizushima J and Yanase S. The nonaxisymmetric instability of the wide-gap spherical Couette flow. Phys. Fluids, 1997, **9**:1197-1199.

[6] Wimmer M. Experiments on a viscous fluid flow between concentric rotating spheres. J. Fluid Mech., 1976, **78**:317-335.

[7] Yavorskaya I, Belyaev U, Monakhov A *et al.* Stability, nonuniqueness and transition to turbulence in the flow between two rotating spheres. 1980, Rep.595, Space Research Institute of the Academy of Science, USSR.

[8] Nakabayashi K, Tsuchida Y. Flow-history effect on higher modes in the spherical Couette system. J. Fluid Mech., 1995, **295**: 43-60.

[9] Bühler K, Zerip J. Dynamical instabilities and transition to turbulence in spherical gap flows. In *Advances in Turbulence, Proc. 1st Eurpean Turbu. Conf.* (ed. G. Comte-Bellot & J. Mathieu) Springer, 1987, p.16.

[10] Bartels F. Taylor vortices between two-concentric rotating spheres. J. Fluid Mech., 1982, **119**:1-65.

[11] Marcus P and Tuckerman L. Simulations of flow between two concentric rotating spheres, J. Fluid Mech., 1987, **185**:1-65.

[12] Yuan L, Fu D X and Ma Y W. Numerical study of bifurcation solutions of spherical Taylor-Couette flow. Sci. China Ser. A, 1996, **39**:187-196.

[13] Schrauf G. The first instability in spherical Couette flow. J. Fluid Mech., 1986, **166**:287-303.

[14] Mamun C, Tuckerman L. Asymmetry and Hopf bifurcation in spherical Couette flow. Phys. Fluids, 1994, **7**(1):80-91.

[15] Dumas G and Leonard A. A divergence-free spectral expansions method for three-dimensional flows in spherical-gap geometries. J. Comput. Phys. , 1994,**111**:205-219.

[16] Zikanov O Y. Symmetry-breaking bifurcations in spherical Couette flow. J. Fluid Mech., 1996, **310**:293-324.

[17] Sha W and Nakabayashi K. On the structure and formation of spiral Taylor-Görtler vortices in spherical Couette flow. J. Fluid Mech., 2001, **431**:323-345.

[18] Yuan L. Comparison of implicit multigrid schemes for three-dimensional incompressible flows. J. Comput. Phys., 2002, **177**:134-155.

[19] Rogers S and Kwak D. Upwind differencing scheme for the time-accurate incompressible Navier-Stokes equations, AIAA J., 1990, **28**:253.

[20] Ladyzhenskaya O A. Mathematical analysis of Navier-Stokes equations for incompressible liquids. Ann. Rev. Fluid Mech., 1975, **7**:249-272.

[21] Schroeder W and Keller HB. Wavy Taylor-vortex flows via multigrid-continuation methods. J. Comput. Phys., 1990, **91** (1):197-227.

(a) 1-vortex flow   (b) 2-vortex flow

Figure 1: Meridional streamlines for steady 1- and 2-vortex flows, $\beta = 0.06, Re = 3080$. Solid lines are in counterclockwise while dotted lines are in clockwise directions.
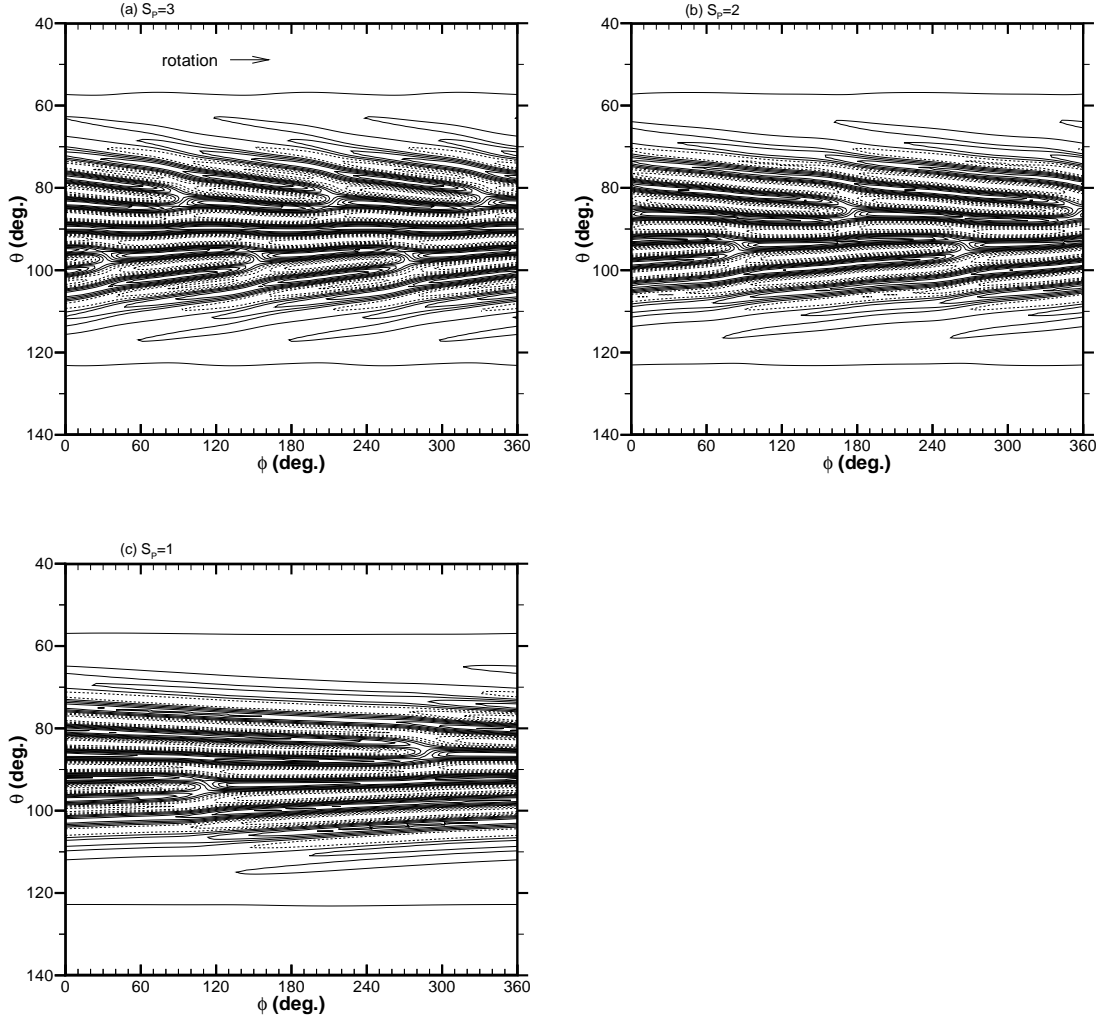
Figure 2: Radial velocity contours in the $(\phi - \theta)$ spherical surface at the radial position $r = R_1 + 0.5\beta$ for the three different spiral TG vortex flows, $Re = 3300, \beta = 0.06$. The three flow states are (a) IITS($S_{\mathrm{P}} = 3$), (b) IITS($S_{\mathrm{P}} = 2$) and (c) IITS($S_{\mathrm{P}} = 1$). Solid lines are for $v_r \geq 0$, while dashed lines for $v_r < 0$.

11
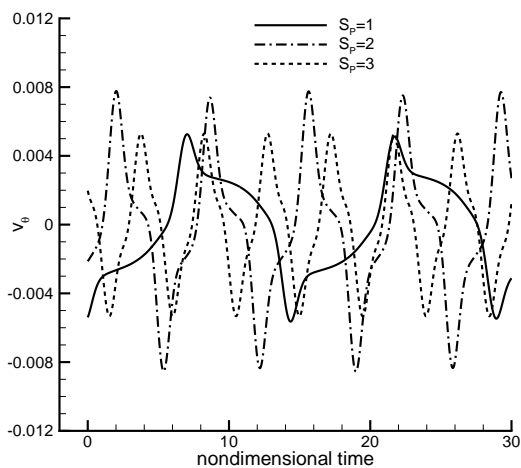
Figure 3: Time history of the circumferential velocity component at the equator. The fundamental period for $S_P = 1, 2$ and 3 are 14.70, 6.825 and 4.483, respectively, and represents time for each disturbance to pass by a stationary observer. The period of rotation of the spiral TG vortex flow T_s is counted between three consecutive peak intervals for $S_P = 3$, and between two peak intervals for $S_P = 2$. The rotation frequency of the spiral TG vortex is obtained as $f_S/f_0 = T_S/T_0$, where $T_0 = 2\pi/\Omega_1$. $\beta = 0.06, Re = 3300$
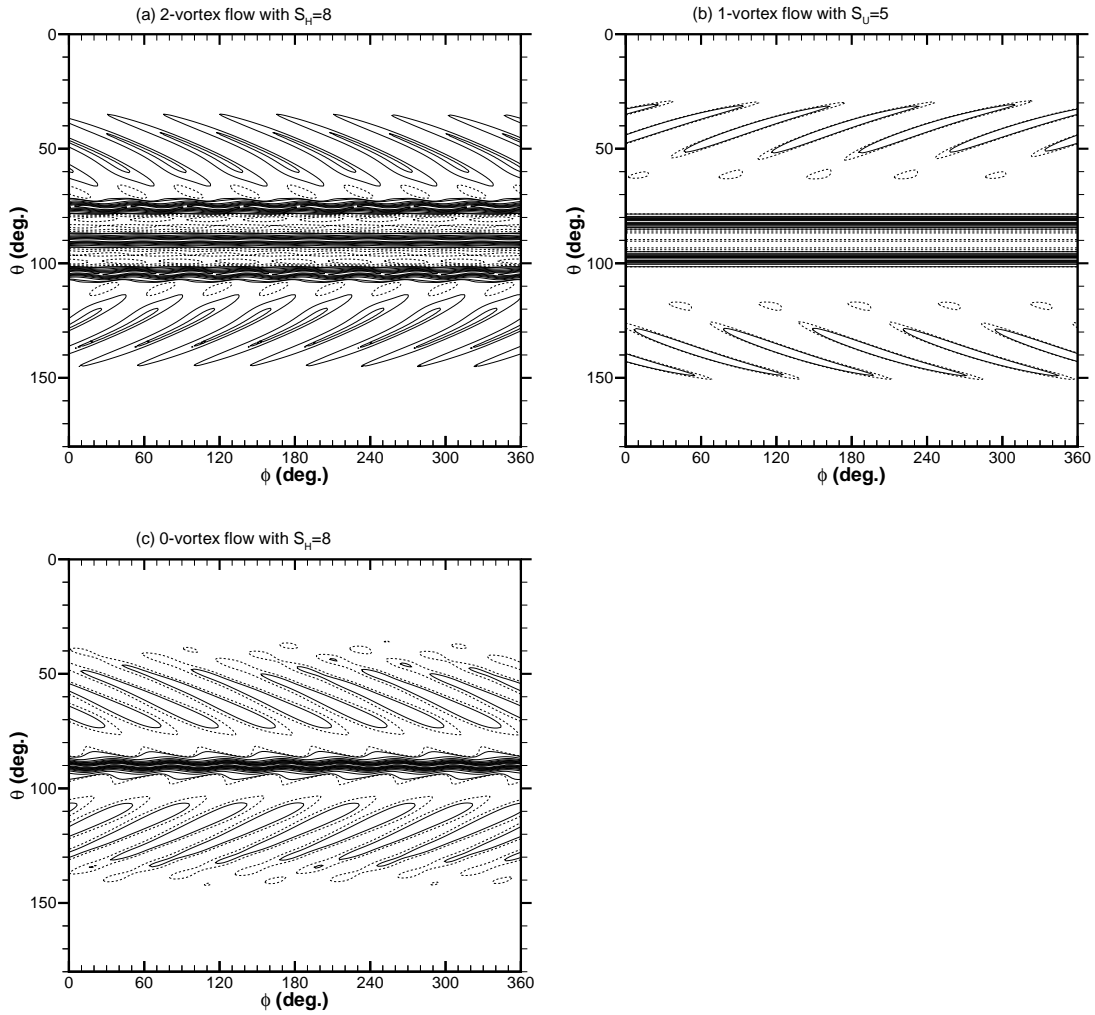
Figure 4: Radial velocity contours in the $(\phi - \theta)$ spherical surface at $r = R_1 + 0.7\beta$ for three periodic flow states in $\beta = 0.18, Re = 7200$. Solid lines are for $v_r \geq 0$, while dashed lines for $v_r < 0$.
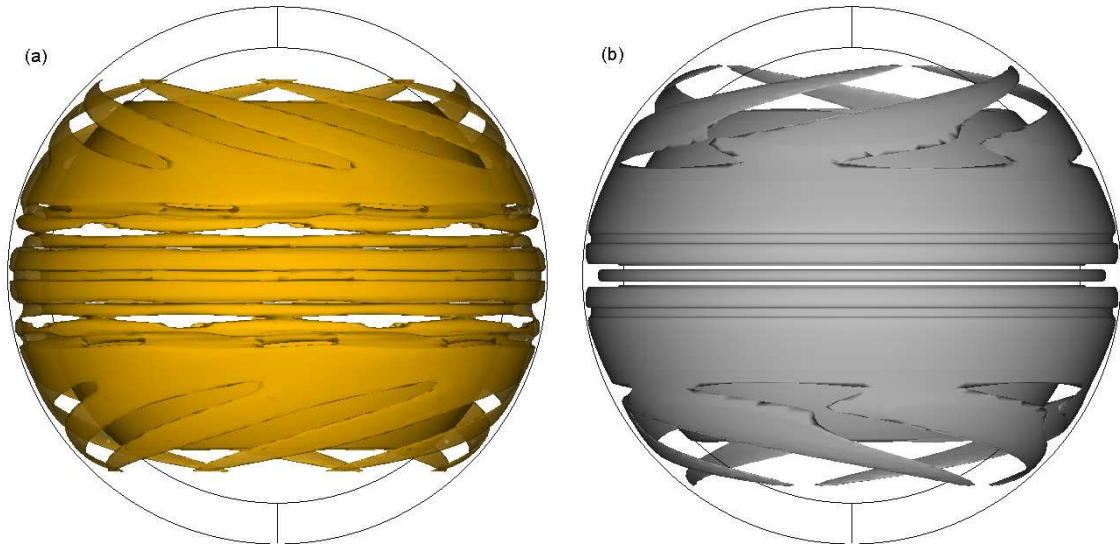
Figure 5: Isosurfaces of meridional velocity $v_m = \sqrt{v_r^2 + v_\theta^2} = 0.114$ for (a) 2-vortex flow with shear waves $S_H = 8$, and (b) 1-vortex flow with Stuart vortices $S_U = 5$, $\beta = 0.18$, $Re = 7200$.